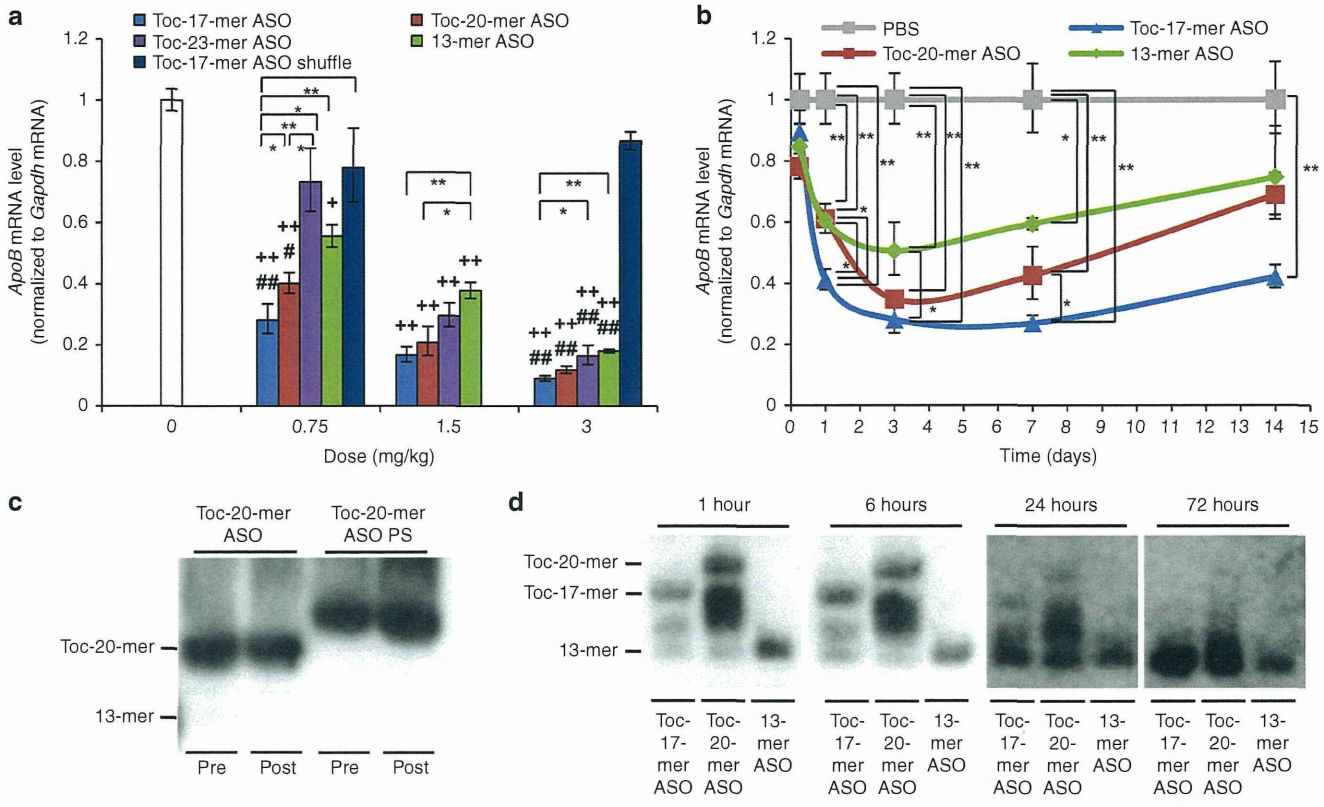

Figure 3 Dose-dependent reductions in mRNA levels and time course of gene silencing by intravenous injection of Toc-ASOs. (**a**) Dose-dependent reduction of gene by intravenous injection of Toc-ASOs. Quantitative RT-PCR analyses of *Apolipoprotein B* (*ApoB*) mRNA levels relative to *gapdh* mRNA levels in 3 days after injection of 0.75, 1.5 or 3 mg/kg Toc-ASOs. The data shown are relative to those from mice that received PBS alone and are presented as mean values ± SEM ($n = 3$, $^{+}P < 0.05$, $^{++}P < 0.01$ versus PBS, $^{\#}P < 0.05$, $^{\#\#}P < 0.01$ versus Toc-17-mer ASO shuffle, and $^{*}P < 0.05$, $^{**}P < 0.01$ between each groups). (**b**) Duration of gene silencing by intravenous injection of Toc-ASOs. Quantitative RT-PCR analyses of *Apolipoprotein B* (*ApoB*) mRNA levels relative to *gapdh* mRNA levels in the liver 6 hours, 1, 3, 7, and 14 after injection of 0.75 mg/kg Toc-ASOs. The data shown are relative to those from mice that received PBS alone and are presented as mean values ± SEM ($n = 3$, $^{*}P < 0.05$, $^{**}P < 0.01$). (**c**) The stability of Toc-ASOs. Toc-20-mer ASO and Toc-20-mer ASO PS were incubated in mouse serum with protease inhibitor for 24 hours at 37 °C. The samples were estimated by northern blot analysis to detect 13-mer gapmer sequences of Toc-ASO. (**d**) Northern blot analysis to detect 13-mer gapmer sequences of Toc-ASO in the liver 1 hour to 3 days after injection of mice with 0.75 mg/kg of each ASOs.

mice. The respective ED_{50} values for Toc-17-mer ASO, Toc-20-mer ASO, Toc-23-mer ASO, and 13-mer ASO were 24, 60, 145, and 216 nmol/kg. This indicating that Toc-17-mer ASO, Toc-20-mer and Toc-23-mer ASO were more efficacious than 13-mer ASO. We then examined the time courses of their effects. Mice were injected with 0.75 mg/kg of these α-tocopherol–conjugated ASOs, and their livers were collected from 6 hours to 14 days after injection. The gene silencing effects of 13-mer ASO, Toc-17-mer ASO, and Toc-20-mer ASO were observed 1 day after injection. The Toc-17-mer and Toc-20-mer ASOs showed significantly stronger than 13-mer ASO gene silencing effects from days 3 to 14 and days 3 to 7, respectively (**Figure 3b**).

Next, in order to know whether the Toc-ASOs were cleaved before or after reaching the liver, stability studies were performed on Toc-20-mer ASO and Toc-20-mer ASO PS. Both of the Toc-ASOs were incubated in mouse serum with protease inhibitor for 24 hours at 37 °C. In northern blot analysis to detect ASO, both Toc-20-mer-ASO and Toc-20-mer-ASO PS were stable 24 hours after incubation with mice serum (**Figure 3c**). We then examined *in vivo* analysis and performed northern blot analysis to detect ASO. Mice were injected with 0.75 mg/kg of Toc-ASOs, and their livers were collected at 1, 6, 24, and 72 hours after injection. The several bands including the full length of Toc-17-mer and Toc-20-mer ASOs were observed at 24 hours or earlier time point of after injection, and only 13-mer ASOs were detected at 72 hours after injection of Toc-17-mer and Toc-20-mer ASOs (**Figure 3d**). These results suggested that Toc-17-mer ASO and Toc-20-mer ASOs reached the liver with full length, and then were cleaved to 13-mer ASO.

In vivo pharmacokinetics

To determine whether Toc-ASOs was predominantly distributed to liver in mouse after intravenous injection, the *in vivo* tissue accumulation of Toc-ASOs was examined for 6 hours after intravenous injection of Toc-ASOs labeled with Alexa Fluor 647 at the 3′-ends. The accumulation of Toc-ASOs in the mouse liver was ~3.5-fold higher than that of α-tocopherol–unconjugated ASOs while the accumulation of Toc-ASOs in the mouse kidney was approximately six-fold lower than that of α-tocopherol–unconjugated ASOs

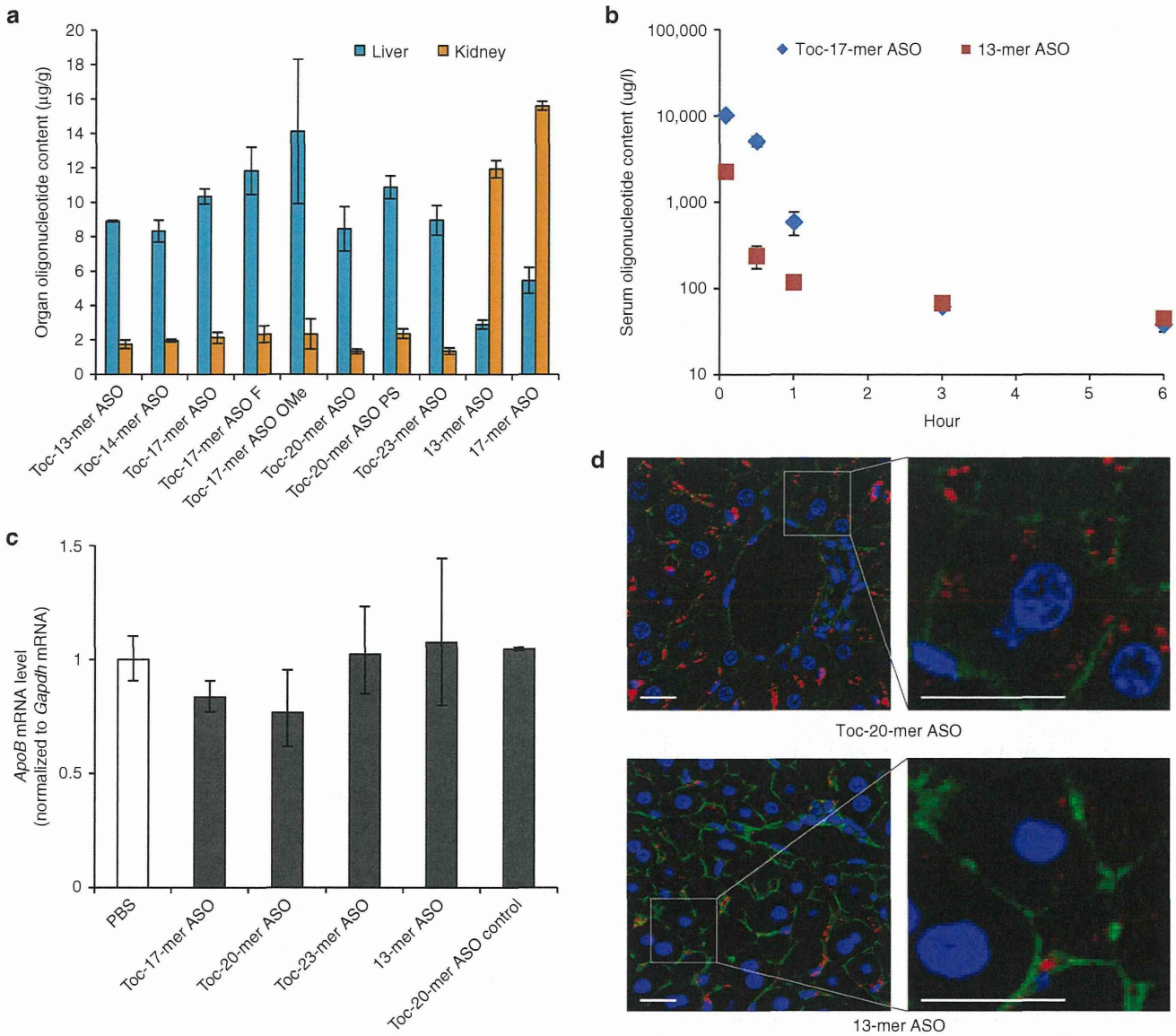

Figure 4 Biodistribution and pharmacokinesis of Toc-ASO. (**a**) Measurement of ASO concentrations in each organ 6 hours after injection of 3 mg/kg Alexa Fluor 647–labeled ASOs. The data shown are presented as mean values ± SEM ($n = 3$). The other organs including brain, heart, lung, spleen, intestine and muscle had no signal. (**b**) Measurement of serum ASO concentration 5 minutes to 6 hours after injection of mice with 3 mg/kg of Alexa Fluor 647–labeled ASOs. The data shown are presented as mean values ± SEM ($n = 3$). N.D., not detected. (**c**) Quantitative RT-PCR analyses of *Apolipoprotein B* (*ApoB*) mRNA levels relative to *gapdh* mRNA levels in the intestine 3 days after injection of 3 mg/kg Toc-ASOs. The data shown are relative to those from mice that received PBS alone and are presented as mean values ± SEM ($n = 3$). (**d**) Confocal laser images of mouse liver sections taken 6 hours after injection of 3 mg/kg Alexa Fluor 647–labeled Toc-ASOs. Red, Alexa Fluor 647–labeled ASO; green, Alexa Fluor 488 Phalloidin; blue, Hoechst 33342; Bar = 20 μm.

(**Figure 4a**). No accumulation of Toc-ASOs or α-tocopherol–unconjugated ASOs was observed in brain, heart, lung, spleen, intestine, and muscle because of under detection limit. These results suggest the predominantly delivery of Toc-ASOs to liver after intravenous injection compared to α-tocopherol–unconjugated ASOs.

Figure 4b shows the serum concentration-time profiles of Toc-17-mer ASOs and 13-mer ASO after intravenous injection in mice (3 mg/kg). The serum concentration of Toc-17-mer ASOs was greater at 5, 30, and 60 minutes after injection than that of 13-mer ASO in mice while there is no difference at 3 hours after injection between serum concentrations of Toc-17-mer ASOs and 13-mer ASO in mice. As shown in **Table 2**, the area under the serum concentration-time curve (AUC) of Toc-17-mer ASOs was 4.21-fold greater than that of 13-mer ASO in mice. Total body clearance (CLtot), mean residence time (MRT), steady-state volume of distribution (Vdss) and initial elimination rate constant (K_α) of Toc-17-mer ASOs was lower than that of 13-mer ASO in mice (**Table 2**). There is no significant change of the terminal elimination rate constant (K_β) between Toc-17-mer ASOs and 13-mer ASO in mice. These results suggested systemic clearance of Toc-17-mer ASO was significantly reduced compared to α-tocopherol–unconjugated ASOs 13-mer ASO, and

Table 2 Pharmacokinetic parameters of Toc-17-mer ASO and 13-mer ASO after 3 mg/kg intravenous administration

	Toc-17-mer ASO	13-mer ASO
AUC(∞) μg/ml·minute	379±14**	90±11
CLtot (ml/minute/g)	0.0079±0.0005**	0.0374±0.0025
MRT (minute)	32±1**	165±30
Vdss (ml/g)	0.252±0.023**	6.12±0.76
K_α (minute^{-1})	0.0571±0.0041**	0.1200±0.0111
K_β (minute^{-1})	0.00272±0.00137	0.00303±0.00052

The pharmacokinetic parameters were determined by model-independent moment analysis according to experimental procedures.
AUC, area under the serum concentration-time curve; CLtot, total body clearance; MRT, mean residence time; K_α, initial elimination rate constant; K_β, terminal elimination rate constant; Vdss, steady-state volume of distribution. $n = 3$, $^{**}P < 0.01$, significantly different between Toc-17-mer ASO and 13-mer ASO.

Toc-17-mer ASO was delivered to liver from the serum more than that of 13-mer ASO in mice (**Table 2**).

Since *ApoB* mRNA was expressed in the intestinal tract, we measured the *ApoB* mRNA silencing effect of Toc-ASOs in intestine. Toc-ASOs had no silencing effect of target gene in intestine even injected 3 mg/kg to the mice (**Figure 4c**). We also examined the delivery to the liver histologically. We found much more intense Alexa Fluor 647 signals in the cytosol of hepatocytes as well as in the sinusoids of mice injected with Toc-20-mer ASO than in those of mice injected with 13-mer ASO (**Figure 4d**).

Phenotypic analyses of mice using α-tocopherol–conjugated ASOs

The reduction in liver *ApoB* mRNA led to a decrease in serum LDL-cholesterol level. Injection of Toc-17-mer ASO or Toc-20-mer ASO achieved a significant reduction in serum LDL-cholesterol and total cholesterol levels (**Figure 5a**). Western blot analysis of the sera also revealed a clear decrease in ApoB100 content by administration of Toc-17-mer ASO and Toc-20-mer ASO than 13-mer ASO (**Figure 5b**).

Lack of side effects of α-tocopherol–conjugated ASOs

Biochemical analysis of the serum transaminases 3 days after injection of 3 mg/kg ASOs (**Figure 6a**) revealed no marked abnormalities. In addition, no histological abnormalities were found in the livers of 3 mg/kg Toc-17-mer ASO–injected mice (**Figure 6b**).

Discussion

We previously showed that conjugation of α-tocopherol to siRNA (Toc-siRNA) improves the gene silencing effect of this construct *in vivo*;[17] however, here, we found that the direct conjugation of α-tocopherol to ASO (Toc-13-mer ASO) abolished this ability (**Figure 2a**). Because we observed more accumulation of Toc-13-mer ASO than of α-tocopherol–unconjugated 13-mer ASO in the liver (**Figure 4a**), we thought that α-tocopherol attenuated the effect of ASO in the hepatocytes. We therefore inserted second wing between the 5′-end of the ASO and the α-tocopherol to avoid α-tocopherol influence. We chose PEG (hexaethylene glycol) or second wings of nucleic acid analogues (*e.g.*, UNA, 2′-F RNA or

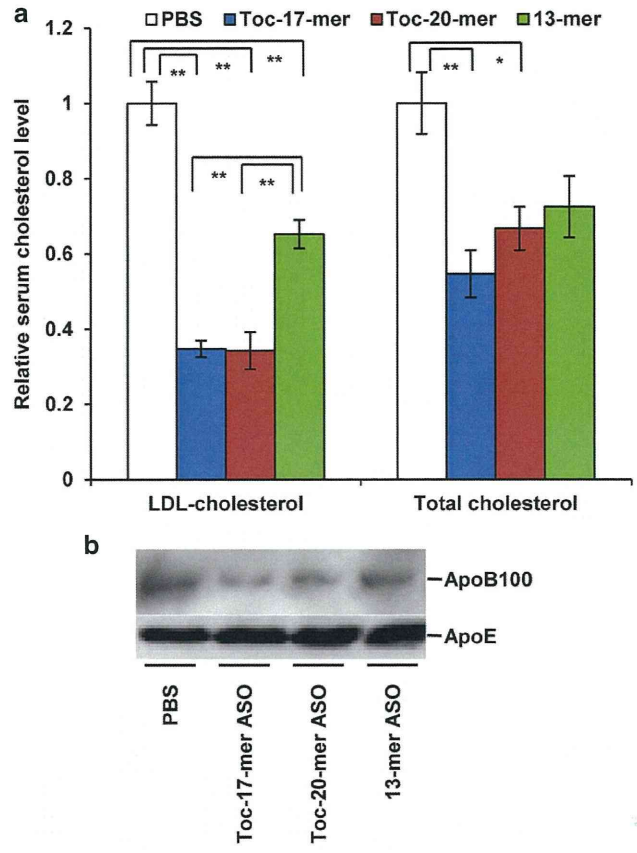

Figure 5 Phenotypic changes in lipid metabolism caused by inhibition of liver *ApoB* mRNA expression. (**a**) Decreased levels of serum low density lipoprotein cholesterol (LDL-cholesterol) and total cholesterol after injection of Toc-ASOs. Sera were collected from mice 3 days after the injection of Toc-ASOs. The resultant ratios were normalized against values from mice that were treated with PBS alone. $n = 3$, data shown are mean values ± SEM. $^{*}P < 0.05$, $^{**}P < 0.01$ compared with the PBS group. (**b**) Western blot analysis to detect serum ApoB100 proteins in mouse serum 3 days after injection.

2′-*O*-methyl RNA) as linkers. Whereas Toc-13-mer, Toc-13-mer PEG, and Toc-20-mer ASO PS had no effect, inserting the second wing of nucleic acid analogues with a natural phosphodiester internucleotide linkage produced a profound gene slicing effect (**Figure 2a**).

Northern blot analysis of the liver from effective Toc-ASO groups showed 13-mer bands (**Figure 2d,e**). Toc-13-mer ASO, Toc-13-mer ASO PEG, and Toc-14-mer ASO could not be observed in northern blot analysis, even though it was certain that the nucleic acids had reached the liver at 6 hour after injection as same amount as Toc-17-mer ASO or Toc-20-mer ASO from the fluorescence measurement (**Figure 4a**). This may have been because the conjugated α-tocopherol inhibited the hybridization of the ASO and the target mRNA when α-tocopherol was too close to the ASO. This clearly indicated that the 13-mer ASO was separated from α-tocopherol by cleavage of the second wing portion, suggesting that silencing of the Toc-ASOs may have been brought about by these cleaved 13-mer ASOs. ASOs bound to α-tocopherol via UNA were not degraded in mice serum (**Figure 3c**). α-tocopherol and second wings of Toc-ASOs were suggested to be cleaved

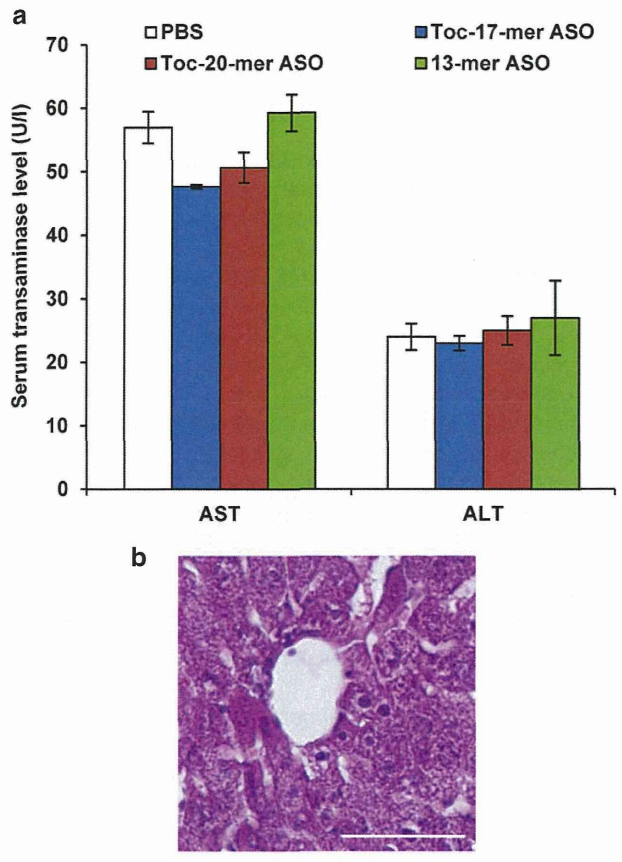

Figure 6 Evaluation of adverse events. (**a**) Serum transaminase levels 3 days after injection of 3 mg/kg Toc-ASOs. $n = 3$, data shown are mean values ± SEM. (**b**) Histopathological analyses of liver from Toc-ASO-injected mouse. Liver sections were prepared 3 days after injection of 3 mg/kg Toc-20-mer ASO.

into 13-mer ASO in mice liver (**Figure 3d**). The high effectiveness of Toc-ASOs in liver appears to be dependent on their high-level, *in vivo* delivery to the liver by α-tocopherol and release from α-tocopherol after uptake by the hepatocytes.

Tissue distribution and pharmacokinetic of Toc-17-mer ASO is different from that of 13-mer ASO (**Figure 4a,b**). Toc-17-mer ASO was predominantly distributed to liver in mice after intravenous injection. The CLtot of Toc-17-mer ASO was significantly reduced in mice compared to that of 13-mer ASO. These findings suggested that conjugation of α-tocopherol significantly improved the pharmacokinetic profile of ASO.

Toc-13-mer PEG's linker, hexaethylene glycol, was designed to be similar in length to that of the 7-mer oligonucleotide second wing of Toc-20-mer ASO. Both probably uncleaved Toc-13-mer PEG and Toc-20-mer ASO PS (Toc-ASOs with phosphodiesterase-resistant second wings) had no gene-silencing effects, indicating that α-tocopherol conjugation inhibited the effect of the ASO and that merely introducing space between α-tocopherol and the 13-mer ASO does not improve the silencing effect of Toc-ASOs.

Conjugation of α-tocopherol barely changed the *Tm* values of Toc-ASOs (**Table 1**), indicating that α-tocopherol conjugation did not markedly affect the duplex formation of ASO with the target mRNA *in vitro*. However, *in vivo*, the high hydrophobicity of α-tocopherol may have impeded gene silencing by interfering with the Toc-ASO's access to the target RNA during its intracellular trafficking by either binding to the membranes of intracellular organelles or intracellular proteins or inhibiting the function of proteins necessary for gene expression (including RNase H), or both.

Toc-17-mer ASO with the UNA second wing was more effective than Toc-17-mer ASO OMe or Toc-17-mer ASO F (**Figure 2a**). Since the arrival amounts to the liver of Toc-17-mer ASO, Toc-17-mer ASO OMe, or Toc-17-mer ASO F were not different so much (**Figure 4a**), the difference of the effects are not considered to be due to the quantity in the liver. Northern blot analysis showed a band signal for the 13-mer ASO in the sample containing the Toc-17-mer ASO with the UNA second wing (**Figure 2d**), and it suggested that the UNA second wing with phosphorothioate bond was more easily cleaved than the 2′-*O*-Me or the 2′-F second wing in hepatocytes.

When we consider the relationship between the efficiency of the Toc-ASO with the phosphate-bound UNA second wing and the length of the second wing, we see that the efficiency was highest for the Toc-17-mer ASO and attenuated for the Toc-ASO with the longer second wing. In contrast, the Toc-14-mer ASO was not effective (**Figure 2b**). Given that we did not observe a 13-mer band in the northern blot with the Toc-14-mer ASO (**Figure 2d**), it may be that the Toc-14-mer ASO's α-tocopherol was not cleaved from the ASO. Therefore, a single UNA may not be enough to be recognized by nucleases. We thought of three possible reasons why the longer second wing attenuated the Toc-ASO's efficacy: (i) it took more time to cleave the longer second wing and (ii) the longer second wing became an obstacle for recognition by the phosphodiesterase.

The RNase H cleavage–mediated silencing mechanism of the gapmer ASO dramatically improved the effectiveness of the ASO. The nucleotide analogues that served as wings (**Figure 1**), such as LNA, MOE, or cET, have been investigated to further increase the effectiveness of the gapmer. Optimization of gapmers (the length of the gap and the wings) has been shown to increase their effectiveness; the wing-gap-wing gapmer nucleotide composition of 2-8-3 or 2-8-2 in the LNA,[13] 5-10-5 (Mipomersen) in MOE,[12] and 3-10-3 in cET[19] were all reported to be excellent. We used the 2-8-3 13-mer ASO, which was one of the most effective LNA-containing gapmers. However, because the amount of unconjugated 13-mer ASO that reached the kidney was higher than that reaching the liver, the 13-mer ASO could not fully exert a sufficient effect in the liver, the target organ (**Figure 4a**). Here, we succeeded in improving the amount of ASO delivered to the liver by binding a delivery molecule to the ASO.

There have been several recent reports of organ-specific delivery of molecules conjugated to siRNA, including cholesterol to the liver[20] or brain capillary endothelial cells,[21] GalNac to the liver,[22] atelocollagen to the liver,[23] dynamic polyconjugates to the liver,[24] peptide derived from rabies virus glycoprotein to neurons,[25] and oligo-9-arginine peptide to T cells,[26] as well as the delivery of peptide conjugated to phosphorodiamidate morpholino oligomers to skeletal muscle.[27] Recently,

Prakash *et al.* reported GalNac conjugated to ASO with linker, and the GalNac-conjugated ASO improved potency in mouse liver resulted in enhanced ASO delivery to hepatocytes.[28] The GalNac-conjugated ASO is metabolized to liberate the parent ASO in the liver,[28] similar to Toc-ASO.

Our chimeric ASO with the appropriately cleavable second wing can be applied to different organs or cells by selecting different delivery molecules. Further improvements of the molecule design of the second wing will help further potency and safety for the clinical application of this new type of chimeric oligonucleotide.

Materials and methods

Design and synthesis of ASOs. A series of DNA-LNA gapmers of different lengths (13- to 23-mers) were designed to target mouse *ApoB* mRNA (NM_009693).[13] The ASOs were synthesized by Gene Design (Osaka, Japan). The sequences of the ASOs targeting *ApoB* mRNA were as follows: 13-mer ASO, 5′-G*C*a*t*t*g*g*t*a*t*T*C*A-3′; Toc-13-mer ASO PEG, 5′-**X***PEG*G*C*a*t*t*g*g*t*a*t*T*C*A-3′; Toc-13-mer ASO, 5′-**X**G*C*a*t*t*g*g*t*a*t*T*C*A-3′; 14-mer ASO, 5′-*A*G*C*a*t*t*g*g*t*a*t*T*C*A-3′; Toc-14-mer ASO, 5′-**X***A*G*C*a*t*t*g*g*t*a*t*T*C*A-3′; 17-mer ASO, 5′-*UCCA*G*C*a*t*t*g*g*t*a*t*T*C*A-3′;Toc-17-merASO,5′-**X***UCCA*G*C*a*t*t*g*g*t*a*t*T*C*A-3′; Toc-17-mer ASO F, 5′-**X***UCCA*G*C*a*t*t*g*g*t*a*t*T*C*A-3′; Toc-17-mer ASO OMe, 5′-**X**UCCAG*C*a*t*t*g*g*t*a*t*T*C*A-3′; Toc -20-mer ASO PS, 5′-**X***A*A*G*U*C*C*A*G*C*a*t*t*g*g*t*a*t*T*C*A-3′; 20-mer ASO, 5′-*AAGUCCA*G*C*a*t*t*g*g*t*a*t*T*C*A-3′; Toc-20-mer ASO, 5′-**X***AAGUCCA*G*C*a*t*t*g*g*t*a*t*T*C*A-3′; and Toc-23-mer ASO, 5′-**X***AUAAAGUCCA*G*C*a*t*t*g*g*t*a*t*T*C*A-3′. The shuffle sequence of the ASO targeting *ApoB* mRNA was as follows: Toc-17-mer ASO shuffle, 5′-**X***UCCA*C*G*a*t*t*g*g*t*a*t*C*G*C; The sequence of the ASO targeting human *TTR* mRNA (NM_000371) was as follows:Toc-20-mer ASO control, 5′-**X***TGTTTTA*T*G*t*c*t*c*t*g*c*c*T*G*G-3′; The sequence of the ASO targeting SRB1 mRNA (NM_000371) was as follows: Toc-17-mer ASO control, 5′-**X***GCUUC*A*g*t*c*a*t*g*a*c*T*T*C-3′; where the asterisks represent phosphorothioate linkages, the upper case boldface letter X represents α-tocopherol, the upper case italicized letters represent UNA, the lower case letters represent DNA, the underlined characters represent 2′-*O*-methyl sugar modification, the underlined upper case italicized letters represent 2′-Fluoro modification, and the upper case letters represent LNA (capital C denotes LNA methylcytosine). Alexa Fluor 647 fluorophores were covalently bound to the 3′-ends of the ASOs, and α-tocopherol was covalently bound to the 5′-ends of the ASOs.

UV melting analyses. UV absorbance versus temperature profile measurements were performed with an eight-sample cell changer, in quartz cells of 1-cm path length. The variations with temperature in the differences in UV absorbance measured at wavelengths of 260 nm and 320 nm were monitored. The samples containing the oligonucleotides with the complementary RNA, 5′-ugaauaccaaugcuggacuuuauaaccaatc-3′, (1.25 μmol/l in PBS) were first rapidly heated to 90 °C, maintained at 90 °C for 10 minutes, and then allowed to cool to 0 °C at a rate of 0.5 °C/minute. These samples were then left at 0 °C for 30 minutes, and the dissociation was recorded by heating to 90 °C at a rate of 0.5 °C/minute.

Mouse studies. Wild type Crlj:CD1 (ICR) mice or C57BL/6 mice aged 4–5 weeks (Oriental Yeast, Tokyo, Japan) were kept on a 12-hour light/dark cycle in a pathogen-free animal facility with free access to food and water. ASOs were administered to the mice via tail vein injection based upon body weight (0.75–6 mg/kg). All oligonucleotides were formulated in PBS, which also served as the control. The oligonucleotides were administered via either a single injection or repeated injections. All animal experiments were performed with more than three mice, and all procedures were carried out according to Tokyo Medical and Dental University's ethical and safety guidelines for animal experiments (#0140144A). Sera were collected 3 days after the final injection to measure LDL-cholesterol levels and for western blot analysis. For postmortem analyses, mice were deeply anesthetized with intraperitoneally administered 60 mg/kg pentobarbital and then sacrificed by transcardiac perfusion with PBS after confirming the absence of the blink reflex.

Quantitative real-time polymerase chain reaction. Total RNA was extracted from mouse liver or intestine by using Isogen (Nippon Gene, Tokyo, Japan). To detect mRNA, DNase-treated RNA (2 μg) was reverse-transcribed with SuperScript III and Random Hexamers (Life Technologies, Carlsbad, CA). To detect short RNAs, including DNA-LNA gapmer, quantitative RT-PCR analysis was performed by using a TaqMan MicroRNA Reverse Transcription Kit (Applied Biosystems, Foster City, CA) and a Light Cycler 480 Real-Time PCR Instrument (Roche Diagnostics, Mannheim, Germany). The primers and probes for the DNA/LNA gapmers and mouse *ApoB*, *Gapdh* (NM_008084), *Ttr* (NM_013697), *Sod1* (NM_011434), and *Hprt* (NM_013556) genes were designed by Applied Biosystems.

Isolation of the lipoprotein fraction from serum. The LDL fraction was prepared by ultracentrifugation according to a previously published method,[21] with modification. First, a half-volume of a solution of density 1.182 g/ml was layered onto one volume of mouse serum and centrifuged for 3.6 hours at 337,000*g* at 16 °C. The half-volume of the upper solution was set aside for use in experiments as the LDL fraction.

Western blot analysis. The LDL fraction from mouse serum samples (2 μl) was diluted with 18 μl of PBS, mixed with 5 μl of Laemmli sample buffer (Bio-Rad, Hercules, CA), and then denatured at 95 °C for 2 minutes. Total proteins were separated by electrophoresis on a 5–20% gradient polyacrylamide gel (ATTO Corporation, Tokyo, Japan) and transferred onto polyvinylidene difluoride membranes. Blots were probed with goat primary antibodies against ApoE (1:500, sc-6384, Santa Cruz Biotechnology, Santa Cruz, CA) and ApoB (1:500, sc-11795, Santa Cruz Biotechnology), and then incubated with an anti-goat secondary antibody (1:2,000, sc-2020, Santa Cruz Biotechnology) conjugated with horseradish

peroxidase. Blots were visualized with SuperSignal West Femto Maximum Sensitivity Substrate (Thermo Fisher Scientific, Waltham, MA) and analyzed by use of a ChemiDoc System (Bio-Rad).

Northern blot analysis. Total RNA was extracted from mouse liver by using Isogen II (Nippon Gene). Total RNA (30 μg) was separated by electrophoresis through an 18% polyacrylamide-urea gel and transferred to a Hybond-N^+ membrane (Amersham Biosciences, Piscataway, NJ). The blot was hybridized with a probe corresponding to the ASO sequence. The sequence of the probe for detecting ASO was 5′-TGAataccaatGC-3′; the lower case letters represent DNA, and the upper case letters represent LNA (capital C denotes LNA methylcytosine). The digoxigenin-ddUTP was covalently bound to the 5′-end of the ASO probe. The signals were visualized with a Gene Images CDP-star Detection Kit (Amersham Biosciences).

Evaluation of blood chemistry. A single 0.75 mg/kg dose of ASOs in PBS was injected into the tail vein of mice. Sera were collected 3 days after injection, and blood chemistry was assessed.

Nuclease stability assays. Nuclease stability assays were performed according to a previously published method[29] with a modification. Briefly, ASOs were incubated in mouse serum with protease inhibitor for 24 hours at 37 °C. RNA was extracted using Isogen II, and were examined by northern blot analysis.

Measurement of ASO concentration in each organ. Mice were injected with Alexa Fluor 647–labeled ASOs; 6 hours later, tissues were obtained from various organs (brain, heart, lung, liver, kidney, spleen, intestine, and muscle). Tissues were homogenized in 500 μl of phosphate-buffered saline (PBS, Sigma-Aldrich, St Louis, MO). The concentration of Alexa Fluor 647 was measured by using i-control (Tecan, Männedorf, Switzerland).

Plasma pharmacokinetic studies. Each mouse received a bolus intravenous injection of Alexa Fluor 647–labeled Toc-17-mer ASO or Alexa Fluor 647–labeled 13-mer ASOs into tail vein. Blood samples were collected at indicated times (5, 30, 60, 180, and 360 minutes). The serum concentration of Alexa Fluor 647 was measured by using i-control (Tecan). The plasma concentration versus time data were analyzed by MOMENT based on the model-independent moment analysis method.[30] The nonlinear least-squares regression analysis program MULTI.[31] The pharmacokinetics parameters such as area under the serum concentration-time curve (AUC), the total body clearance (CLtot), the mean residence time (MRT) and the steady-state volume of distribution (Vdss), elimination rate constants (K_α and K_β) were calculated as described previously.[32]

Histopathological analyses. For pathological analyses, mouse liver was collected 3 days after injection and then postfixed in 4% paraformaldehyde in PBS for 6 hours, embedded in paraffin, cut into 4-μm thick sections with a Leica CM 3050 S cryostat (Leica Microsystems, Wetzlar, Germany), and stained with hematoxylin and eosin (Muto Pure Chemicals, Tokyo, Japan). The slides were analyzed under an Olympus AX80 Automatic Research Photomicroscope (Olympus, Tokyo, Japan). To analyze the distribution of ASO in the liver, 0.75 mg/kg Alexa Fluor 647–labeled ASOs in PBS was injected into mouse tail veins. Mouse liver was collected 3 days after injection, fixed in 4% paraformaldehyde in PBS for 12 hours, and then snap-frozen in liquid nitrogen. Tissue sections (10 μm) were prepared with a Leica CM3050 S cryostat (Leica Microsystems). The sections were stained with Hoechst 33342 (Sigma-Aldrich) to visualize nuclei and with 13 nmol/l Alexa Fluor 488 phalloidin (Life Technologies) to visualize cell membranes. They were then analyzed under a LSM 510 confocal microscope (Carl Zeiss MicroImaging GmbH).

Statistical analysis. All data represent means ± SEM. Student's two-tailed *t*-tests were used to determine the significance of differences between two groups in quantitative RT-PCR assays, analyses of lipoprotein levels in serum and plasma pharmacokinetic studies. One-way ANOVA followed by Tukey's test were used for multiple comparisons between pairs of groups.

Acknowledgments. This study was supported by grants from the Core Research for Evolutional Science and Technology (CREST), the Japan Science and Technology Agency (JST), Japan (to T.Y.), the Ministry of Health, Labor, and Welfare, Japan (to T.Y.), and Shionogi & Co., Ltd. This work was done in Bunkyo-ku, Tokyo, Japan. The investigators received funding from Shionogi & Co., Ltd. The authors declare no conflict of interest.

1. Kole, R, Krainer, AR and Altman, S (2012). RNA therapeutics: beyond RNA interference and antisense oligonucleotides. *Nat Rev Drug Discov* **11**: 125–140.
2. Obika, S, Nanbu, D, Hari, Y, Morio, K, In, Y, Ishida, T *et al.* (1997). Synthesis of 2′-O,4′-C-methyleneuridine and -cytidine. Novel bicyclic nucleosides having a fixed $C_{3'}$, *-endo* sugar puckering. *Tetrahedron Lett* **38**: 8735–8738.
3. Obika, S, Nanbu, D, Hari, Y, Andoh, J, Morio, K, Doi, T *et al.* (1998). Stability and structural features of the duplexes containing nucleoside analogues with a fixed N-type conformation, 2′-O,4′-C-methyleneribonucleosides. *Tetrahedron Lett* **39**: 5401–5404.
4. Singh, SK, Koshkin, AA, Wengel, J and Nielsen, P (1998). LNA (locked nucleic acids): synthesis and high-affinity nucleic acid recognition. *Chem Commun* **4**: 455–456.
5. Freier, SM and Altmann, KH (1997). The ups and downs of nucleic acid duplex stability: structure-stability studies on chemically-modified DNA:RNA duplexes. *Nucleic Acids Res* **25**: 4429–4443.
6. Martin, P (1995). Ein neuer Zugang zu 2′-O-Alkylribonucleosiden und Eigenschaften deren Oligonucleotide. *Helv Chim Acta* **78**: 486–504.
7. Seth, PP, Vasquez, G, Allerson, CA, Berdeja, A, Gaus, H, Kinberger, GA *et al.* (2010). Synthesis and biophysical evaluation of 2′,4′-constrained 2′O-methoxyethyl and 2′,4′-constrained 2′O-ethyl nucleic acid analogues. *J Org Chem* **75**: 1569–1581.
8. Murray, S, Ittig, D, Koller, E, Berdeja, A, Chappell, A, Prakash, TP *et al.* (2012). TricycloDNA-modified oligo-2′-deoxyribonucleotides reduce scavenger receptor B1 mRNA in hepatic and extra-hepatic tissues–a comparative study of oligonucleotide length, design and chemistry. *Nucleic Acids Res* **40**: 6135–6143.
9. Monia, BP, Lesnik, EA, Gonzalez, C, Lima, WF, McGee, D, Guinosso, CJ *et al.* (1993). Evaluation of 2′-modified oligonucleotides containing 2′-deoxy gaps as antisense inhibitors of gene expression. *J Biol Chem* **268**: 14514–14522.
10. Wahlestedt, C, Salmi, P, Good, L, Kela, J, Johnsson, T, Hökfelt, T *et al.* (2000). Potent and nontoxic antisense oligonucleotides containing locked nucleic acids. *Proc Natl Acad Sci USA* **97**: 5633–5638.
11. Jiang, K (2013). Biotech comes to its 'antisenses' after hard-won drug approval. *Nat Med* **19**: 252.
12. Crooke, ST and Geary, RS (2013). Clinical pharmacological properties of mipomersen (Kynamro), a second generation antisense inhibitor of apolipoprotein B. *Br J Clin Pharmacol* **76**: 269–276.

13. Straarup, EM, Fisker, N, Hedtjärn, M, Lindholm, MW, Rosenbohm, C, Aarup, V *et al.* (2010). Short locked nucleic acid antisense oligonucleotides potently reduce apolipoprotein B mRNA and serum cholesterol in mice and non-human primates. *Nucleic Acids Res* **38**: 7100–7111.
14. Koller, E, Vincent, TM, Chappell, A, De, S, Manoharan, M and Bennett, CF (2011). Mechanisms of single-stranded phosphorothioate modified antisense oligonucleotide accumulation in hepatocytes. *Nucleic Acids Res* **39**: 4795–4807.
15. Juliano, RL, Ming, X and Nakagawa, O (2012). Cellular uptake and intracellular trafficking of antisense and siRNA oligonucleotides. *Bioconjug Chem* **23**: 147–157.
16. Kappus, H and Diplock, AT (1992). Tolerance and safety of vitamin E: a toxicological position report. *Free Radic Biol Med* **13**: 55–74.
17. Nishina, K, Unno, T, Uno, Y, Kubodera, T, Kanouchi, T, Mizusawa, H *et al.* (2008). Efficient *in vivo* delivery of siRNA to the liver by conjugation of alpha-tocopherol. *Mol Ther* **16**: 734–740.
18. Uno, Y, Piao, W, Miyata, K, Nishina, K, Mizusawa, H and Yokota, T (2011). High-density lipoprotein facilitates *in vivo* delivery of a-tocopherol-conjugated short-interfering RNA to the brain. *Hum Gene Ther* **22**: 711–719.
19. Hung, G, Xiao, X, Peralta, R, Bhattacharjee, G, Murray, S, Norris, D *et al.* (2013). Characterization of target mRNA reduction through in situ RNA hybridization in multiple organ systems following systemic antisense treatment in animals. *Nucleic Acid Ther* **23**: 369–378.
20. Soutschek, J, Akinc, A, Bramlage, B, Charisse, K, Constien, R, Donoghue, M *et al.* (2004). Therapeutic silencing of an endogenous gene by systemic administration of modified siRNAs. *Nature* **432**: 173–178.
21. Kuwahara, H, Nishina, K, Yoshida, K, Nishina, T, Yamamoto, M, Saito, Y *et al.* (2011). Efficient *in vivo* delivery of siRNA into brain capillary endothelial cells along with endogenous lipoprotein. *Mol Ther* **19**: 2213–2221.
22. Kanasty, R, Dorkin, JR, Vegas, A and Anderson, D (2013). Delivery materials for siRNA therapeutics. *Nat Mater* **12**: 967–977.
23. Takeshita, F, Minakuchi, Y, Nagahara, S, Honma, K, Sasaki, H, Hirai, K *et al.* (2005). Efficient delivery of small interfering RNA to bone-metastatic tumors by using atelocollagen in vivo. *Proc Natl Acad Sci USA* **102**: 12177–12182.
24. Rozema, DB, Lewis, DL, Wakefield, DH, Wong, SC, Klein, JJ, Roesch, PL *et al.* (2007). Dynamic PolyConjugates for targeted *in vivo* delivery of siRNA to hepatocytes. *Proc Natl Acad Sci USA* **104**: 12982–12987.
25. Kumar, P, Wu, H, McBride, JL, Jung, KE, Kim, MH, Davidson, BL *et al.* (2007). Transvascular delivery of small interfering RNA to the central nervous system. *Nature* **448**: 39–43.
26. Kumar, P, Ban, HS, Kim, SS, Wu, H, Pearson, T, Greiner, DL *et al.* (2008). T cell-specific siRNA delivery suppresses HIV-1 infection in humanized mice. *Cell* **134**: 577–586.
27. Jearawiriyapaisarn, N, Moulton, HM, Buckley, B, Roberts, J, Sazani, P, Fucharoen, S *et al.* (2008). Sustained dystrophin expression induced by peptide-conjugated morpholino oligomers in the muscles of mdx mice. *Mol Ther* **16**: 1624–1629.
28. Prakash, TP, Graham, MJ, Yu, J, Carty, R, Low, A, Chappell, A *et al.* (2014). Targeted delivery of antisense oligonucleotides to hepatocytes using triantennary N-acetyl galactosamine improves potency 10-fold in mice. *Nucleic Acids Res* **42**: 8796–8807.
29. Lennox, KA and Behlke, MA (2010). A direct comparison of anti-microRNA oligonucleotide potency. *Pharm Res* **27**: 1788–1799.
30. Tabata, K, Yamaoka, K, Kaibara, A, Suzuki, S, Terakawa, M and Hata, T (1999) Moment analysis program available on Microsoft Excel®. *Xenobio Metab Dispos* **14**: 286–293.
31. Yamaoka, K, Tanigawara, Y, Nakagawa, T and Uno, T (1981). A pharmacokinetic analysis program (multi) for microcomputer. *J Pharmacobio-dyn* **4**: 879–885.
32. Nishida, Y, Ito, S, Ohtsuki, S, Yamamoto, N, Takahashi, T, Iwata, N *et al.* (2009). Depletion of vitamin E increases amyloid beta accumulation by decreasing its clearances from brain and blood in a mouse model of Alzheimer disease. *J Biol Chem* **284**: 33400–33408.

神経内科
研修ノート

シリーズ総監修
永井良三　自治医科大学学長

責任編集
鈴木則宏　慶應義塾大学教授

編集
荒木信夫　埼玉医科大学教授
神田　隆　山口大学教授
吉良潤一　九州大学教授
塩川芳昭　杏林大学教授
西野一三　国立精神・神経医療研究センター
神経研究所部長
水澤英洋　国立精神・神経医療研究センター
病院院長

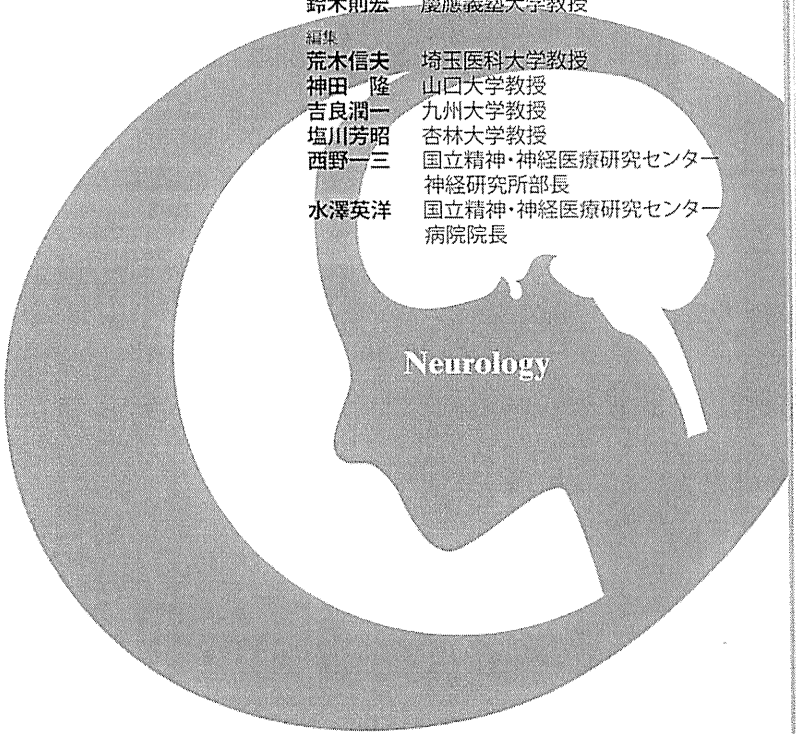

診断と治療社

9 プリオン病

DOs

- □ プリオン病には孤発性，遺伝性，獲得性の3種類がある．
- □ 最も多いのは古典型孤発性 Creutzfeldt-Jakob 病であり，約7割を占めている．急速進行性の認知症，四肢のミオクローヌス，小脳失調，錐体路徴候，錐体外路徴候，3～6か月で無動性無言に至る経過が特徴的である．
- □ MRI 拡散強調画像上の大脳皮質と基底核の高信号，脳波上の周期性同期性放電(PSD)などを呈する．
- □ 臨床症状，画像・髄液検査，遺伝子検索により的確な診断を下すことが重要である．

1 基本的な考え方

急速進行性の認知症症状とミオクローヌスなどを特徴とする．五類感染症に指定されており，医師は診断後7日以内に保健所へ報告する．孤発性，遺伝性，獲得性の3種類があり，最も多いのは，典型的な経過をとる古典型孤発性 Creutzfeldt-Jakob 病(CJD)である(表1)．

2 疫 学

発症率は人口100万人あたり年間1人程度で，平均年齢は67.1歳である．わが国の特徴は獲得性や遺伝性の割合が相対的に多く，獲得性プリオン病のほとんどが硬膜移植による CJD という点である．

3 臨床症状

a 孤発性 CJD ……

ヒト・プリオン病の約8割を占める．約7割の典型例は古典型とよばれ，急速進行性の認知症，ミオクローヌス，小脳失調，視覚異常，さらに錐体路・錐体外路症状等が出現し，平均3～6か月で無動性無言に陥る．全経過はわが国の場合，1～2年程度である．孤発性のなかには比較的緩徐に進行する例もある．診断基準を表2に示す．

b 遺伝性プリオン病……

PrP 遺伝子の変異に起因し，多数の変異が知られている．常染色体優性遺伝であるが，家族歴がほとんどない病型もあり，わが国ではむしろそのような症例が多い．症候(表現型)により，遺伝性 CJD，Gerstmann-Sträussler-Scheinker 病(GSS)，致死性家族性不眠症(FFI)に大別される(表1)．病初期が緩徐進行性で Alzheimer 病のような経過をとる症例や，小脳症状が強く脊髄小脳変性症様の経過の症例，Parkinson 症候群，末梢神経障害で発症する症例などもある．

c 獲得性プリオン病……

大半が硬膜移植例で，古典型 CJD 様の病型と，失調性歩行障害で発症し比較的緩徐に進行し脳波の周期性同期性放電(PSD)を欠く病型もある．

表1 ヒト・プリオン病の分類(わが国での頻度)

①**特発性プリオン病**(76.7%)
- A)孤発性 Creutzfeldt-Jakob 病(CJD)
  - (ア)古典型，あるいは Heidenhain 型；MM1/MV1
  - (イ)失調型；VV2, MV2(クール一斑 variant)
  - (ウ)視床型(致死性孤発性不眠症；FSI, MM2 視床型)；MM2
  - (エ)大脳皮質型；MM2(MM2 皮質型)，VV1

②**遺伝性(家族性)プリオン病**(19.6%)
- A)遺伝性(家族性)CJD
- B)Gerstmann-Sträussler-Scheinker 病(GSS)
- C)致死性家族性不眠症(FFI)
- D)その他

③**獲得性(感染性)プリオン病**(3.7%)
- A)クール一病
- B)医原性 CJD(乾燥硬膜，脳外科手術，深部脳波電極，角膜移植，ヒト成長ホルモン，ヒト・ゴナドトロピン)
- C)変異型 CJD

4 病態生理

正常プリオン蛋白の立体構造(コンフォメーション)が変化し，伝播性を有する異常プリオン蛋白に変化し，中枢神経系に蓄積して神経細胞変性を起こす．コンフォメーション変化や神経細胞毒性のメカニズムの詳細はわかっていない．

表2 孤発性 Creutzfeldt-Jakob 病の診断基準

①**確実例**：特徴的な病理所見，またはウエスタンブロット法や免疫染色法で脳に異常プリオン蛋白が検出されたもの．

②**ほぼ確実例**：病理所見や異常プリオン蛋白の証明は得られていないが，進行性認知症を示し，脳波にて周期性同期性放電(PSD)を認める．さらに，ミオクローヌス，視覚または小脳症状，錐体路または錐体外路徴候，無動性無言の4項目中2項目以上を満たすもの，あるいは，「③疑い例」に該当し，髄液 14-3-3 蛋白陽性で全臨床経過が2年未満であるもの．

③**疑い例**：ほぼ確実例と同様の臨床症状を呈するが，脳波上 PSD がなく臨床経過が2年未満のもの．

5 診 断

『プリオン病診療ガイドライン 2014』が厚生労働省研究班により発刊されている(http://prion.umin.jp/guideline/guideline_2014.pdf)．

a 脳 MRI ……

拡散強調画像または FLAIR 画像で大脳皮質，基底核(被殻，尾状核)，症例によっては視床にも高信号を認める(図1)．

b 脳 波……

病初期には徐波化・不規則化がみられ，ミオクローヌスが出現する頃に PSD(図2)が出現し，末期には PSD は消失し脳波は平坦化する．

c 髄液検査……

外観，細胞数は通常は正常で，蛋白量についてもほとんどの症例で正常である．14-

図1 古典型孤発性 Creutzfeldt-Jakob 病の脳 MRI 拡散強調画像
拡散強調像が最も感度が高く，大脳皮質および基底核に高信号を認める．

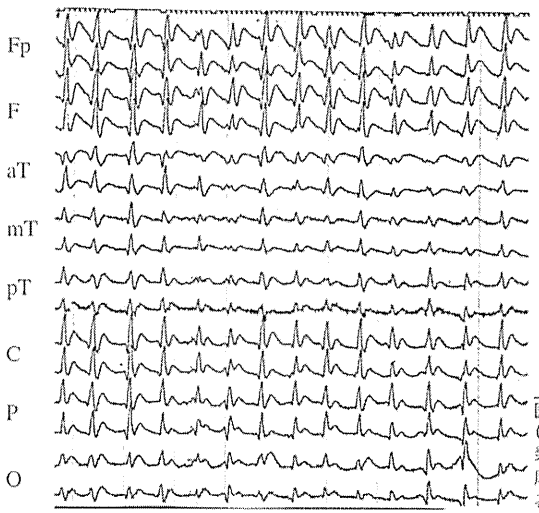

図2　周期性同期性放電(PSD)の脳波
発作性高振幅徐波が，一定の周期で大脳全般に出現している．

3-3蛋白と総タウ蛋白が増加する．近年，real-time qucking-induced conversion(RT-QUIC)法により髄液中の PrP^{Sc} の検出が可能となっている．

6 治　療

根本治療は確立されておらず，対症的，支持的治療が主となる．特定疾患治療研究事業対象疾患であり，医療費助成を受けられる．通常の診療行為で感染する危険はないので，差別的対応にならないように心掛ける．新たな治療薬の開発として，プリオン蛋白の異常化阻止などの治療薬の開発が進められている．

Pitfall

非典型的な経過をとり，髄液検査も陰性の症例も存在するので，そのような症例では，検査結果で否定せずに，総合的に診断する必要がある．

7 感染対策

プリオン病は発症後のみならず潜伏期間においても感染危険部位に接触した医療器具，さらには変異型CJD(vCJD)において血液を介して伝播する．プリオン病患者に使用した手術器具に対して，現在推奨されている消毒・滅菌方法を表3に示した(http://prion.umin.jp/guideline/cjd_2008all.pdf)．

表3　プリオン対応滅菌方法

①焼却可能な器具，用具はすべて焼却する．
②器具に付着した血液・組織片をできる限り取り除いた後，3%SDS溶液にて3～4分間100℃煮沸し，手作業またはウォッシャーディスインフェクターによる洗浄後にプレバキューム方式のオートクレーブで134℃ 10分処置する．
③軟性内視鏡などの加圧・加熱処理ができない手術器具に関しては適切な洗浄剤による十分な洗浄後に過酸化水素低温ガスプラズマ滅菌による洗浄・不活化処理する．
④病理標本に関しては90%ギ酸で1時間処理すること．

Pitfall

14-3-3蛋白やRT-QUIC法による PrPSc は痙攣後症候群，低酸素脳症等で偽陽性例になる場合があり注意が必要である．

DON'Ts

- □ 髄液を扱うときや脳外科手術時の器具は，プリオン対応でない滅菌をしてはいけない．
- □ 髄液検査やMRI画像が陽性の場合でも痙攣，低酸素脳症，自己免疫性脳炎などの鑑別をせずにプリオン病と診断してはいけない．

文献

1) Nozaki I, et al: Brain 2010; 133: 3043-3057
2) 厚生労働科学研究費補助金難治性疾患克服研究事業「プリオン病及び遅発性ウイルス感染症に関する調査研究班」編，プリオン病と遅発性ウイルス感染症，金原出版，東京，2010

東京医科歯科大学大学院医歯学総合研究科 脳神経病態学(神経内科)　三條伸夫